Crystallographic orientation and electrode nature are rate determining factors for the electric power generation by *Geobacter sulfurreducens*

Beatriz Maestro[a1*], Juan M. Ortiz[a2], Germán Schrott[b], Juan P. Busalmen[b], Víctor Climent[a] and Juan M. Feliu[a]

[a] *Instituto Universitario de Electroquímica. Universidad de Alicante. Apdo. 99, Alicante E-03080, Spain.*
[b] *Área de electroquímica y corrosión, INTEMA (CONICET). Juan B. Justo 4302, B7608FDQ Mar del Plata, Argentina.*
[1]*Present address: Instituto de Biología Molecular y Celular, Universidad Miguel Hernández. Avda Universidad s/n, Elche, 03202, Spain.*
[2]*Present address: Aqualia Integrated Water Management SA. Madrid, Spain.*

** Corresponding author. E-mail: bmaestro35@gmail.es. Telephone: (+34) 966658474 Fax: +34 966658758*

E-mail addresses: juanmanuel.ortiz1@fcc.es (J.M. Ortiz), *germans@fi.mdp.edu.ar* (G. Schrott), *jbusalme@fi.mdp.edu.ar* (J.P. Busalmen), *clicvic@gmail.com* (V. Climent), *juan.feliu@ua.es* (J.M. Feliu).

Abstract

We have investigated the influence of electrode material and crystallographic structure on electron transfer and biofilm formation of *Geobacter sulfurreducens.* Single-crystal gold - Au(110), Au(111), Au(210) - and platinum - Pt(100), Pt(110), Pt(111), Pt(210) - electrodes were tested and compared to graphite rods. *G. sulfurreducens* electrochemically interacts with all these materials with different attachment kinetics and final current production, although redox species involved in the electron transfer to the anode are virtually the same in all cases. Initial bacterial colonization was fastest on graphite up to the monolayer level, whereas gold electrodes led to higher final current densities. Crystal geometry showed to have an important influence, with Au(210) sustaining a current density of up to 1442 (±101) μA cm^{-2} at the steady state, over Au(111) with 961 (±94) μA cm^{-2} and Au(110) with 944 (±89) μA cm^{-2}. On the other hand, the platinum electrodes displayed the lowest performances, including Pt(210). Our results indicate that both crystal geometry and electrode material are key parameters for the efficient interaction of bacteria with the substrate and should be considered for the design of novel materials and microbial devices to optimize energy production.

Keywords: *Geobacter sulfurreducens*; single-crystal electrode; biofilm; electron transport; cytochrome

1. Introduction

The mechanisms for current production by electro-active microorganisms colonizing anode surfaces are the subject of thorough investigation due to their implication in the development of bioelectrochemical systems such as the promising technology of microbial fuel cells (MFC) [1]. In the anode of these devices, dissolved organic matter is oxidized by electro-active microorganisms that possess the outstanding ability of using an electrode as the final electron acceptor. After extracting the energy required for growth, these cells transfer the produced electrons to outer membrane cytochromes (OMC's), and finally to the anodic surface through an extracellular electron transfer chain whose structure and function remain to be elucidated in detail [2]. Several bacterial genera have the ability to colonize electrodes and use them as electron acceptors [3]. Among such microorganisms, strains from the *Geobacter* genera typically dominate the natural bacterial populations colonizing electrodes [4]. *Geobacter sulfurreducens* is the most efficient current producer described so far (see [4] for a review) and is one of the few microbes that have been found to completely oxidize organic compounds to carbon dioxide using an electrode as the sole electron acceptor [5].

Many molecular biology studies have focused on the external electron transfer (EET) mechanisms in *G. sulfurreducens* biofilms, providing relevant information about participating molecules and identifying OmcZ, OmcB and OmcS cytochromes as playing a relevant role [6-8]. Moreover, electrochemical and spectroelectrochemical approaches have demonstrated that external cytochromes in this strain are responsible for the reaction of charge transfer to the electrode surface [9, 10], but the full identity of the molecules acting in this step is still unknown. For the octaheme cytochrome OmcZ, a formal potential of -0.22 V *vs.* standard hydrogen electrode (SHE) (corresponding to -0.42 V *vs.* Ag/AgCl) has been estimated [11] with a very broad potential window from -0.42 to -0.06 V *vs*. SHE arising from its multiheme composition. The hexaheme cytochrome OmcS has an apparent equilibrium potential of -0.21 V *vs.* SHE (corresponding to -0.41 V *vs.* Ag/AgCl) with a reduction potential range from -0.36 to -0.04 V *vs.* SHE [12]. Finally, the redox potential of the dodecaheme OmcB has been estimated to be centered at -0.19 V *vs.* SHE (corresponding to -0.39 V vs Ag/AgCl) [13].

G. sulfurreducens does not require soluble mediators to generate a high current density, but external cytochromes must establish a molecular interaction with the electrode to allow direct electron transfer (DET) [9, 10]. In DET of isolated protein systems, an optimal electronic coupling between the electrode and the molecular redox center is necessary for electron tunnelling to occur. Among many factors, this coupling is mostly dependent on the orientation of adsorbed proteins [14], and in turn on variables such as pH, ionic strength [15] and electrode surface topography and charge [16]. Therefore, it should not be surprising that the structure, topology, functionalization and surface charge of the anode material could play a decisive influence on the initial bacterial attachment step and on the electrochemical function of the biofilm. On the other hand, the influence of the mineral (oxyhydr)oxide composition and crystallinity on reduction rates by *Geobacter* and *Shewanella* species has been a subject of controversy. Roden [17] suggested that oxide reduction is not strongly controlled by oxide crystal thermodynamic properties, but mainly by the surface area. However, other authors have highlighted the impact of chemical and crystallographic orientation of the

surface [18-20]. In these studies, the authors present the respiration rates by normalized area, and show that poorly crystalline materials such as amorphous Fe(III) (oxyhydr)oxide or feroxyhyte are better electron acceptors than other minerals which present a more crystalline structure, as goethite and hematite. Moreover, they indicate that minerals with the same chemical composition differ on Fe(III) reduction rates in the same way, depending on their relative crystallinity.

Single-crystal electrodes may provide an unequivocal answer to the question of whether the structural properties of the electrode surface affect DET in *Geobacter* systems. These electrodes are characterized by a precise atomic arrangement on their surface, leading to a well-distinct electrochemical reactivity. The structure of the interfacial region between these electrode surfaces and the electrolytic solution has been characterized with great detail in the past and, therefore, they offer an excellent starting point for the study of the influence of electrode structural properties on biofilm electroactivity. Among the different properties characterizing the electrochemical behaviour of metal surfaces, the potential of zero charge (pzc) plays a very important role. This parameter represents the value of the potential where the charge separation at the interphase vanishes, therefore allowing the definition of a rational correlation between the electrode potential and the sign and magnitude of charge at the interface. As a last advantage, single-crystal surfaces present a well-defined surface area that allows an unambiguous determination of area-dependent variables, such as current density and charge accumulation.

In this work, we have comparatively tested gold and platinum single-crystals with different properties in terms of topology, defectiveness and zero charge potential, aiming at clarifying the influence of the electrode material and surface structure on bacterial attachment, maximum current density generation and the activity of redox species involved in the DET process. Besides, we compare these results to those obtained on graphite, which is the typically used material for analyzing *Geobacter* electrochemistry. Our results show that gold electrodes, and especially Au(210), produce the highest steady state current densities, demonstrating that both material type and surface geometrical configuration exert a strong influence on the EET process.

2. Materials and Methods

2.1. Culture preparation

All reagents were analytical and biochemical grade and were obtained from Sigma-Aldrich. *G. sulfurreducens* used as inoculum to the electrochemical cell was grown in batch mode in culture medium containing 50 mM $NaHCO_3$, 9.4 mM NH_4Cl, 2.6 mM NaH_2PO_4, 30 mM KCl, 10 mL × L^{-1} trace vitamins solution [21] and 10 mL × L^{-1} mineral solution [21]. The pH was adjusted to 7.0, and the medium was supplemented with 0.1 mM sodium citrate, 20 mM sodium acetate and 40 mM sodium fumarate (acceptor limitation conditions), purged with N_2/CO_2 (80 %/20 %) and sterilized in bottles caped with butyl rubber stoppers and secured with a crimped aluminium cap (Bellco Glass Inc). Anaerobic culture was promoted by 1/10 (v/v) inoculum and supported at 30 ºC without shaking for 48 h, until $O.D._{600nm}$ was around 0.6. In the case of culture medium used into the electrochemical cell, no electrode acceptor was added except the polarized electrode.

2.2. Electrode preparation

Three gold single-crystal: Au(111), Au(110), Au(210), four Pt single-crystal: Pt(100), Pt(110), Pt(111), Pt(210) and a graphite rod (TED Pella, Grade 1) were tested as working electrodes. The single-crystals were prepared by melting a high purity gold or platinum wire (99.9998%, Alfa-Aesar), and were subsequently oriented, cut and polished as described elsewhere [22]. Prior to each experiment, each single-crystal electrode was flame-annealed and quenched in ultra-pure water. To check the electrode surface, cyclic voltammetry (CV) was performed in 100 mM $HClO_4$, and the voltammetric profile was compared to those reported in the literature [23, 24]. In order to completely remove the biofilm from the electrodes after each experiment, the gold single-crystals were cleaned by applying a potential of 10 V in 100 mM H_2SO_4 during 10 s, washed with ultra-pure water, then inserted into 1 M HCl and washed again with ultra-pure water. The process was repeated twice. After this, the gold single-crystals were heated in an oven at 860 ºC for 12 h. In the case of platinum electrodes, after overnight washing in nitric acid, they were flame annealed and cooled into clean nitric acid twice, then washed with ultra-pure water, flamed again and quenched in ultra-pure water. The electrode structure was checked by CV each time before a new experiment.

Graphite rods (3 mm diameter, Grade 1 Spec-Pure, TED Pella, Inc., Reddong, CA) (2 cm^2 immersed) were polished using an abrasive disc P1200 (Buehler, Illinois, USA), sonicated in ultra-pure water for 10 min, kept in 1 M NaOH for 30 min, and in 1 M HCl overnight. After each step, graphite rods were washed extensively with ultra-pure water.

2.3. Cell configuration and electrochemical experiments

A custom-made, single-chamber, three-electrode reactor was used to grow biofilms and for all the electrochemical experiments. The counter electrode was a platinum wire and the reference was an Ag/AgCl (3 M NaCl) electrode (RE-5B BASi, USA). The potential of Ag/AgCl (3 M NaCl) electrode vs SHE was checked (+ 0.2 V). The reactor had several holes in which the different working electrodes were fitted to allow biofilm growth on them simultaneously. The single-crystal electrodes were positioned in a meniscus configuration ensuring that only the well-defined surface with the selected crystallographic orientation was making contact with the electrolyte. After assembling and sterilizing the whole system, the tank containing the feeding medium and the reactor were purged overnight with N_2/CO_2 (80 %/20 %) previously filtered through an oxygen filter (Agilent Technologies). The cell was filled with 80 mL growth medium containing 20 mM acetate as the electron donor, and no acceptor other than the polarized electrode. Inoculation was performed by adding 25 % (v/v) of a *G. sulfurreducens* early stationary phase culture ($O.D._{600\ nm}$ 0.6). All the electrodes were simultaneously and independently polarized at +0.2 V using a 8-channel potentiostat (CHI1030B CH Instruments) and current evolution was recorded over time. The system was batch operated for the first 25 h before turning on circulation of the feeding medium at 0.2 mL/min for continuous mode. Temperature was controlled at 30 °C during all the experiment. The electrochemical cell was continuously purged with N_2/CO_2 (80 %/20 %) in the headspace and the medium in the reactor was continuously stirred at low rate. Conductivity at 25 ºC of the initial medium was 4 mS cm^{-1}. Four independent experiments were performed.

2.4. Electrochemical measurements

At different times of growth, the electrochemical activity of adsorbed bacteria was tested by cyclic voltammetry, starting in the anodic direction at +0.2 V and covering a potential range from 0.4 to -0.6 V. While doing this, stirring and pumping of the medium were stopped. The scan rate was 10 mV s^{-1}. A control CV was performed before inoculation to check the absence of current.

2.5. Laser scanning confocal microscopy (LSCM)

At the end of each experiment, the electrodes were carefully removed, washed with fresh medium twice and fluorescently stained with the LIVE/DEAD Baclight bacterial viability kit (Invitrogen) as previously described [25]. In brief, 3 μL of a mixture 1:1 of SYTO 9:propidium iodide was added to 1 mL of culture medium. Electrodes were exposed to this mixture during 15 min at room temperature in the dark before washing with culture medium. Confocal images were captured using an inverse laser scanning confocal microscope (Leika DM IRE2) with 60x oil-immersion lens. In order to obtain a three-dimensional image of the biofilm, multiple optical slices were recorded. The excitation/emission wavelengths for SYTO 9 and propidium iodide were 488/500-550 nm and 543/600-670 nm, respectively. Total (red plus green fluorescent) and metabolically active (green fluorescent) thicknesses of the biofilm were directly measured at four different fields of view and subsequently averaged in each experiment.

3. Results and discussion

3.1. Microbial electricity production and voltammetric characterization of the biofilm on the single-crystal electrodes

Single-crystal electrodes provides a suitable system that allows the precise determination of area-dependent variables, such as current density and charge accumulation, which may be valuable to characterize the electrochemical behaviour of *Geobacter* species. Chronoamperometry of a representative experiment is shown in Fig. 1A. Current production from all electrodes started as soon as bacteria were added, but initial current production was higher and bacteria grew faster on the graphite electrode, showing a doubling time for current production of about 6 h in agreement with previous reports [28]. The high amount of functional groups present at the graphite surface, such as quinones, carboxylic acids and alcohols, can mimic humic substances present in the natural environment of *Geobacter*, facilitating the rapid arrangement of bacteria [29]. After 25 h of incubation, the current produced on graphite and gold electrodes is indicative of a monolayer stage of growth, as determined by Marsili et al. [28]. Among the metallic materials, gold electrodes demonstrated a better performance than platinum ones, with Au(210) displaying the fastest current increase (Fig. 1A), with a doubling time of about 7 h, compared to 10 and 12 h shown by Au(110) and Au(111), respectively. It should be noted that the (210) crystal possesses a very low surface atomic density and the lowest pzc within the gold surfaces [26], thus bearing the most positive charge at +0.2 V, which may facilitate the interaction with negatively charged bacteria. On the other hand, current production on platinum electrodes was very small at

this stage (Fig. 1A, inset), suggesting that bacterial adhesion is hampered by some negative effect that delays the electrode colonization.

Here Table 1
Here Fig. 1

The electrochemical characterization of biofilms developed on the electrodes was performed by cyclic voltammetry at increasing times of growth. The analysis of voltammograms registered at the end of the batch culture step (25 h of growth) shows the turnover signal characteristic of metabolically active cells together with non-catalytic signals with mid-peak potentials of about -0.2 V that change in size and position upon cycling, depending on the electrode material (Fig. 2). The occurrence of these non-catalytic signals is intriguing because they seem to be associated to cytochromes participating in the EET to the electrode [30], but without playing a role in electrode respiration. The expression and presence of these cytochromes at the interface is thought to be a consequence of a programmed response of cells, not directly related to current production. Taking the steady state current level produced by the biofilm as a baseline, a transferred charge of 28, 120 and of 390 μC cm^{-2} can be calculated from the area below non-catalytic oxidation peaks in the first cycle of CV on Au(210), graphite and Au(111) (Fig. 2), respectively. Considering a mean storing capacity of 8 electrons per fully reduced cytochrome (*e.g.*, OmcZ) and a maximum surface coverage of 2.7×10^{-12} mol of proteins per cm^2 of electrode surface [31], a surface coverage density of 3.6×10^{-11}, 1.5×10^{-10} and 5×10^{-10} mol of proteins per cm^2 can be calculated, corresponding to 13, 56 and 185 densely packed cytochrome layers on Au(210), graphite and Au(111), respectively. These values are on the same order of magnitude than those described by Bonanni et al [31] and seem to follow an inverse relation to the current of the biofilms on each material. This gives support to the charge storing role for these molecules and indeed suggests that their expression and accumulation at the interface depends in some way on the suitability of the electrode material as an electron acceptor. On the other hand, changes in the peak size and position of these non-catalytic signals may be the result of variations in the position of external cytochromes as a consequence of the potential scan, which would decrease the number of protein molecules suitably coupled with the electrode. Alternatively, taking into account that microbial cells have been described to partially desorb from the electrode surface upon potential cycling (Kuzume et al, unpublished results), the occurrence of irreversible processes like protein unfolding and/or reductive desorption can not be ruled out either.

Here Fig. 2

Regarding the turnover signals, the comparison between the different metallic electrodes shows that the catalytic wave is much more evident at 25 h on Au(210) and Au(110) than on Au(111), or Pt(100) and Pt(111), consistently with the low current production shown at this stage by platinum electrodes (Fig. 1A). No redox signals were detected on Pt(110),. Finally, the voltammogram recorded on graphite is more reversible, displaying a higher non-catalytic oxidation current than on the Au(210) crystal, in spite of producing a turnover current similar to that measured on this metallic electrode (Fig. 2, see below).

The first derivative analysis of the second cycle of voltammograms in all materials (Fig. 2) reveals one dominant inflection point at around -0.39 V,

corresponding to the catalytic process in current production, and additional smaller signals at about -0.28 and -0.16 V, the position of which slightly varies with the electrode material (Fig. 3). The presence of more than one redox center has been previously described [30, 32]. The results suggest that, in all cases, there is a major redox species involved in EET, together with appended, smaller signals which present slight differences between materials, probably due to minor deviations on the reaction involved.

Here Fig. 3

After 25 h of operation in batch, cultures were changed to continuous mode and operated up to a total of 140 h. A representative current evolution profile is displayed in Fig. 1B to show that the relative performance of electrodes changed with time upon biofilm growth. Although the graphite electrode presented the fastest kinetics in initial current generation (Fig. 1A), it was also the first in reaching the saturation current, at approximately 660 μA cm^{-2} (Table 1). Moreover, all gold electrodes reached appreciable higher values of current density at the steady state, outperforming graphite (Fig. 1B; Table 1). This suggests that, in spite of the initial advantage presented by graphite as electron aceptor up to the monolayer level, highly ordered surfaces such as those of gold electrodes may represent in the longer term better substrates for biofilm structuring and current production (Fig. 1B). In this context crystal geometry turned out to be decisive, with Au(210) sustaining a current density of up to 1442 μA cm^{-2} (Table 1). It should be remarked that the experiments were repeated four times, and in the case of Au(210) three different electrodes were tested.

Platinum electrodes reached the steady state current at longer times and showed the poorest performance in current production (Fig. 1B; Table 1). In spite of this, it is worth to mention that they also served as respiratory substrate for *G. sulfurreducens*. Very few reports have previously analyzed the use of this metal for bacterial attachment. Yi et al [33] showed that the maximum current density obtained by *G. sulfurreducens* on graphite is bigger than on platinum electrodes, an observation that these authors attributed to a higher surface area of the unpolished graphite. However, in our experiments, Pt(111) and Pt(100) crystals demonstrated nearly the same performance efficiency as graphite when the system reached the steady state. The poor performance of Pt(110) compared to the other platinum anodes demonstrates that crystal geometry effectively affects the bacterial electrochemical behaviour. The remarkably slow kinetics and low efficiency of biofilm growth on platinum, when compared with gold single-crystals of the same geometry, suggests a negative effect of the former metal on the bacterial metabolism. As a first explanation, the superior reactivity of platinum in surface catalysis for example, may be deleterious for cell functions by inducing irreversible oxidation of cellular molecules/structures.

In order to test the general influence of the (210) surface geometry we checked the current density obtained with a Pt(210) electrode. Supplementary Fig. 1S shows that current density evolution on Pt(210), although somehow slower than on Pt(100), does not lead to significant differences in the steady state current when compared with the other platinum electrodes (Supplementary Fig. 1S, Table 1). This demonstrates that not only the structure but also the type of electrode material affects both the adhesion and efficient interaction with the substrate.

The cyclic voltammograms recorded from approximately 47 h of biofilm growth show the same sigmoid shape on all materials, which is indicative of the catalysis of acetate oxidation by cells. Fig. 4 shows the CV obtained at the end of the experiment (140 h), when the current density was stabilized. The onset potential appears to be the same for all electrodes (around -0.48 V) attaining in all cases a limiting current of about -0.25 V. The first derivative analysis of the voltammograms shows a symmetrical maximum in all cases, initially centered around -0.39 V for gold and platinum electrodes, and shifting to about -0.35 V upon saturation (Table 1). In the case of graphite, the maximum initially appears at -0.36 V after 47 h of growth, evolving to -0.33 V after 140 h. These results show that the mechanism of electron transfer from cytochromes to the electrode does not change significantly along biofilm growth and that it is typically the same irrespective of the electrode material. Slight changes in the calculated midpoint potential could be ascribed to variations in local conditions at the interface (e.g.: pH decrease). Besides, the calculated midpoint potential of the catalytic redox species (around -0.35 V) is compatible with the participation of any of the external cytochromes of *Geobacter*, i.e. with OmcZ, OmcS and/or OmcB [11-13] that have all been shown to play some role in the electron transfer process (reviewed by Lovley, [2]), thus not allowing their separate electrochemical identification.

Here Fig.4

3.2. LSCM visualization of the biofilm

Once the maximum current density was reached, all the anodes were harvested and biofilms were characterized by LSCM. For this purpose, the anodes were independently stained with the LIVE/DEAD BacLight bacterial viability kit. After labelling, bacteria with intact cell membrane emit green light, whereas those with compromised membrane emit red light. An homogeneous and tightly attached biofilm covered the total area of the anode surface (Fig. 5). Intriguingly, a layer of cells with compromised membrane was observed in almost all cases in the proximity of the electrode surface, underlying a thick layer of healthy cells (green in colour). This phenomenon has been previously shown by other authors [9, 34], but the reasons behind this phenomenon are still unclear. The loss of cell viability does not seem to be related to a negative effect of the CV scans, as the effect also appeared after control experiments without performed voltammetries (data not shown). In any case, membrane compromise does not seem to alter the conductive function of cell envelopes and the surrounding matrix, as indicated by the production of current at high rate on almost all the materials (Fig. 1B). This would confirm previous suggestions that electrons may be transported from outer layers of the biofilm by a molecular pathway (putatively composed by cytochromes) external to the cell membrane, which would be associated to the extracellular polysaccharide network [35]. In this sense, the analysis of the C-terminal moiety of OmcZ by the Phyre^2 server, which identifies distant homologs in the database of proteins with known three-dimensional structure [36], suggests that this protein displays structural similarity with the polysaccharide-binding domain of a sugar binding protein from *Bacteroides ovatus* (PDB code: 3ORJ) (data not shown). Therefore, the OmcZ cytochrome might be important in configuring an effective electron network *in vivo* despite the finding that the C-terminal domain is excised upon *in vitro* purification of the protein [11]. The fact that reactivity is sensitive to surface structure even for a thick biofilm indicates that this inner layer stratum, even with

compromised cells, plays a fundamental role in the electron transfer process from the electrode to the active bacteria.

Here Fig. 5

According to LSCM determinations, the thickness of the biofilm developed on graphite anodes was about 35 μm, much bigger than that on Au(110) and Au(111), that was around 10 μm, and in the same order than that observed on Au(210) (around 30 μm) (Table 1). On platinum anodes biofilms were thinner than those on the other materials, in agreement with the production of lower currents (Table 1). Noteworthily, the produced current is related to the total biofilm thickness in single-crystal electrodes (Supplementary Fig. 2S), displaying a better correlation if only the measured thickness of the metabolically active portion of the biofilm is considered. In both cases the current seems to become independent of thickness beyond approximately 1000 μA cm^{-2}.

3.3. Final remarks

The variables determining the efficiency of a given material as an electronic acceptor in *Geobacter*-based electrochemical systems are mostly unknown. It is well known that the structure of the surface strongly affects the properties of the interphase. In particular, under electrochemical conditions, it has a strong influence on the state of charge of the metal electrode as reflected in the variation of the pzc with the crystallographic orientation (Table 1). In our system, the correlation between pzc and the bacterial electrochemical performance is different for platinum and gold. As shown in Table 1, the most efficient crystal, Au(210), has the more negative potential among the gold electrodes, whereas Pt(111) shows the most positive one within the platinum samples. The effect of electrode charge seems to play a more significant role during the initial stages of bacterial attachment, as the (111) crystals, with the most positive pzc, should encounter more difficulties in attracting the negatively charged bacteria, and accordingly they display the lowest current densities at short times (Fig. 1).

Our results demonstrate that electrode material and surface crystallography are key actors for current generation. One possible explanation is that these factors modulate the correct positioning of the bacterial outer cytochromes. The few previously described reports on the interaction of proteins with defined, single-crystal electrodes support this hypothesis. Thus, it has been demonstrated that insulin binding critically depends on the Au-surface atom topology [37], yielding surface specific interaction patterns in which the more open and reactive Au(110) surface structure supports a much higher adsorption of the protein, as compared to Au(111) and Au(100) [37]. This is in accordance with other authors who have simulated the binding of an engineered gold-binding peptide with gold, also showing that molecular interaction depends on the specific crystallographic surface [38]. In our case, the most efficient surfaces are the gold electrodes, and more specifically the Au(210) crystal. An appreciable chemical effect derives from the low coordination number of surface atoms on the more open surfaces such as the (210) crystals. This low coordination usually implies a higher reactivity that might affect adsorption energies and also rate of electron transfer between redox active proteins and electrode surface. The existence of a chemical effect on protein attachment might also explain the difference between gold and platinum as well as the different effect of the crystallographic orientation on both metals. On the other

hand, steric effects are likely to exert a considerable influence in the accommodation on the electrode of a higher number of catalytic cytochromes in a favourable position per unit surface. The Au(210) plane is the single-crystal plane with the lowest packing density, leading to a very open and reactive structure [39] that it is probably more suited to better associate to the irregular, flexible structure of the cytochrome protein molecules than other smoother gold surfaces. This, in turn, would improve the heterogeneous electron transfer process and consequently the respiration of cells by increasing the number of oxidized cytochromes acting as electron acceptors from the cell in the biofilm, allowing the growth of thicker biofilms.

4. Conclusions

Using a single-crystal approach we have unequivocally demonstrated a direct, area-independent relationship between electrode composition and crystallographic structure on *Geobacter* electric power generation. Although graphite is initially more competent, gold electrodes represent in the long term the most efficient substrates for biofilm structuring and current production. In particular, the Au(210) electrode sustained a maximum current density average value as high as 1442 (±101) μA cm^{-2}. Biofilms grown on platinum substrates showed the slowest current increase and the poorest performance when compared with gold electrodes of the same geometry, suggesting that this material is not optimal for the electron transfer process. On the other hand, the voltammograms recorded at different times of biofilm growth suggest that the kind of cytochromes involved in the electron transfer to the anode are the same in all cases. Further studies on the interaction between OMC's and defined electrode surfaces may open up a wide panoply of possibilities to boost the performance of *Geobacter*-based electrochemical devices by modulating both material type and surface crystallography.

Acknowledgements

We are grateful to Dr. Abraham Esteve-Núñez, who generously provided us the strain *Geobacter sulfurreducens* DL-1, and for excellent scientific discussions. This work was supported by the European Union though the BacWire FP7 Collaboration project (contract #: NMP4-SL-2009-229337).

References

[1] Logan, B.E., 2008. Microbial Fuel Cells, first ed. Wiley and Sons, New Jersey.

[2] Lovley, D.R., 2012. Electromicrobiology. Annu. Rev. Microbiol. 66, 391-409.

[3] Logan, B.E., 2009. Exoelectrogenic bacteria that power microbial fuel cells. Nat. Rev. Microbiol. 7, 375-381.

[4] Lovley, D.R., Ueki, T., Zhang, T., Malvankar, N.S., Shrestha, P.M., Flanagan, K.A., Aklujkar, M., Butler, J.E., Giloteaux, L., Rotaru, A-E., Holmes, D.E., Franks, A.E., Orellana, R., Risso, C., Nevin, K.L., 2011. *Geobacter*: the microbe electric's physiology, ecology, and practical applications. Adv. Microb. Physiol. 59, 1-100.

[5] Bond, D.R., Lovley, D.R., 2003. Electricity production by *Geobacter sulfurreducens* attached to electrodes. Appl. Environ Microbiol. 69, 1548-1555.

[6] Inoue, K., Leang, C., Franks, A.E., Woodard, T.L., Nevin, K.P., Lovley, D.R., 2011. Specific localization of the c-type cytochrome OmcZ at the anode surface in current-producing biofilms of Geobacter sulfurreducensEnviron. Microbiol. Rep. 3, 211-217.

[7] Nevin, K.P., Kim, B-C., Glaven, R.H., Johnson, J.P., Woodard, T.L., Methé, B.A., DiDonato, Jr. R.J., Covalla, S.F., Franks, A.E., Liu, A., Lovley, D.R., 2009. Anode biofilm transcriptomics reveals outer surface components essential for high density current production in *Geobacter sulfurreducens* fuel cells. PLoS ONE 4, e5628.

[8] Richter, H., Nevin, K.P., Jia, H., Lowy, D.A., Lovley, D.R., Tender, L.M., 2009. Cyclic voltammetry of biofilms of wild type and mutant Geobacter sulfurreducens on fuel cell anodes indicates possible roles of OmcB, OmcZ, type IV pili, and protons in extracellular electron transfer. Energy and Environ. Sci. 2, 506-516.

[9] Busalmen, J.P., Esteve-Núñez, A., Berna, A., Feliu, J.M., 2008. C-type cytochromes wire electricity-producing bacteria to electrodes. Angew. Chem. Int. Ed. 47, 4874-4877.

[10] Millo, D., Harnisch, F., Patil, S.A., Ly, H.K., Schröder, U., Hildebrandt, P., 2011. In situ spectroelectrochemical investigation of electrocatalytic microbial biofilms by surface-enhanced resonance Raman spectroscopy. Angew. Chem. Int. Ed. 50, 2625-2627.

[11] Inoue, K., Qian, X., Morgado, L., Kim, B.-C., Mester, T., Izallalen, M., Salgueiro, C.A., Lovley, D.R., 2010. Purification and characterization of OmcZ, an outer-surface, octaheme *c*-type cytochrome essential for optimal current production by *Geobacter sulfurreducens*. Appl. Environ. Microbiol. 76, 3999–4007.

[12] Qian, X., Mester, T., Morgado, L., Arakawa, T., Sharma, M.L., Inoue, K., Joseph, C., Salgueiro, C.A., Maroney, M.J., Lovley, D.R., 2011. Biochemical characterization of purified OmcS, a c-type cytochrome required for insoluble Fe(III) reduction in *Geobacter sulfurreducens*. Biochim. Biophys. Acta 1807, 404-412.

[13] Magnuson, T.S., Isoyoma, N., Hodges-Myerson, A.L., Davidson., G., Maroney, M.J., Geesey, G.G., Lovley, D.R., 2001. Isolation, characterization and gene sequence analysis of a membrane associated 89 kDa Fe(III) reducing cytochrome *c* from *Geobacter sulfurreducens*. Biochem. J. 359, 147-152.

[14] Krzeminski, L., Cronin, S., Ndamba, L., Canters, G.W., Aartsma, T.J., Evans, S.D., Jeuken, L.J.C., 2011. Orientational control over nitrite reductase on modified gold electrode and its effects on the interfacial electron transfer. J. Phys. Chem. B 115, 12607-12614.

[15] Groot, M.T., Merkx, M., Koper, M.T.M., 2007. Reorganization of immobilized horse and yeast cytochrome *c* induced by pH changes or nitric oxide binding. Langmuir 23, 3832-3839.

[16] Leopold, M.C., Bowden, E.F., 2002. Influence of gold substrate topography on the voltammetry of cytochrome *c* adsorbed on carboxylic acid terminated self-assembled monolayers. Langmuir 18, 2239-2245.

[17] Roden, E.E., 2003. Fe(III) oxide reactivity toward biological versus chemical reduction. Environ. Sci. Technol. 37, 1319-1324.

[18] Cutting, R.S., Coker, V.S., Fellowes, J.W., Lloyd, J.R., Vaughan, D.J., 2009. Mineralogical and morphological constraints on the reduction of Fe(III) minerals by *Geobacter sulfurreducens*. Geochim. Cosmochim. Acta 73, 4004-4022.

[19] Lovley, D.R., Phillips, E.J.P., 1986. Organic matter mineralization with reduction of ferric iron in anaerobic sediments. Appl. Environ. Microbiol. 51, 683-689.

[20] Lovley, D.R., Phillips, E.J.P., 1988. Novel mode of microbial energy metabolism: organic carbon oxidation coupled to dissimilatory reduction of iron or manganese. Appl. Environ. Microbiol. 54, 1472-1480.

[21] Balch, W.E., Wolfe, R.S., 1979. Specificity and biological distribution of coenzyme M (2-mercaptoethanesulfonic acid). J. Bacteriol. 137, 256-263.

[22] Clavilier, J., Armand, D., Sun, S.G., Petit, M., 1986. Electrochemical adsorption behaviour of platinum stepped surfaces in sulphuric acid solutions. J. Electroanal. Chem. 205, 267-277.

[23] García-Araez, N., Climent, V., Feliu, J., 2009. Potential-dependent water orientation on Pt(111), Pt(100), and Pt(110), as inferred from laser-pulsed experiments. Electrostatic and chemical effects. J. Phys. Chem. C. 113, 9290-9304.

[24] Rodes, A., Herrero, E., Feliu, J.M., Aldaz, A., 1996. Structure sensitivity of irreversibly adsorbed tin on gold single-crystal electrodes in acid media J. Chem. Soc., Faraday Trans. 92, 3769-3776.

[25] Nevin, K.P., Richter, H., Covalla, S.F., Johnson, J.P., Woodard, T.L., Orloff, A.L., Jia, H., Zhang, M., Lovley, D.R., 2008. Power output and columbic efficiencies from

biofilms of *Geobacter sulfurrerducens* comparable to mixed community microbial fuel cells. Environ. Microbiol. 10, 2505-2514.

[26] Trasatti, S., Lust, E., 1999. The potential of zero charge, in: White, R.E., Bockris, J. O´M., Conway, B.E. (Eds), Modern Aspects of Electrochemistry 33. Kluwer Academic Publishers, New York, pp 1-215.

[27] Climent, V., Gómez, R., Feliu, J.M., 1999. Effect of increasing amount of steps on the potential of zero total charge on Pt(111) electrodes. Electrochim. Acta 45, 629-637.

[28] Marsili, E., Sun., J., Bond., D.R., 2010. Voltammetry and growth physiology of *Geobacter sulfurreducens* biofilms as a function of growth stage and imposed electrode potential. Electroanalysis 22, 865-874.

[29] Crittenden, S.R., Sund, C.J., Summer, J.J., 2006. Mediating electron transfer from bacteria to a gold electrode via a self-assembled monolayer. Langmuir 22, 9473-9476.

[30] Jain, A., Gazzola, G., Panzera, A., Zanoni, M., Marsili, E., 2011. Visible spectroelectrochemical characterization of *Geobacter sulfurreducens* biofilms on optically transparent indium tin oxide electrode. Electrochim. Acta 56, 10776-10885.

[31] Bonanni, P.S., Schrott, G.D., Robuschi, L., Busalmen., J.P., 2012. Charge accumulation and electron transfer kinetics in *Geobacter sulfurreducens* biofilms. Energy and Environ. Sci. 5, 6188-6195.

[32] Katuri, K.P., Kavanagh, P., Rengaraj, S., Leech, D., 2010. *Geobacter sulfurreducens* biofilms developed under different growth conditions on glassy carbon electrodes: insights using cyclic voltammetry. Chem. Commun. 46, 4758-4760.

[33] Yi, H., Nevin, K.P., Kim, B-C., Franks, A.E., Klimes, A., Tender, L.M., Lovley, D.R., 2009. Selection of a variant of *Geobacter sulfurreducens* with enhanced capacity for current production in microbial fuel cells. Biosens. Bioelectron. 24, 3498-3503.

[34] Richter, H., McCarthy, K., Nevin, K., Johnson, J.P., Rotello, V.M., Lovley, D.R., 2008. Electricity generation by *Geobacter sulfurreducens* attached to gold electrodes. Langmuir 24, 4376-4379.

[35] Rollefson, J.B., Stephen, C.S., Tien, M., Bond, D.R., 2011. Identification of an extracellular polysaccharide network essential for cytochrome anchoring and biofilm formation in *Geobacter sulfurreducens*. J. Bacteriol. 193, 1023-1033.

[36] Kelley, L.A., Sternberg, M.J.E., 2009. Protein structure prediction on the Web: a case study using the Phyre server. Nat. Protoc. 4, 363-371.

[37] Welinder, A.C., Zhang, J., Steensgaard, D.B., Ulstrup, J., 2010. Adsorption of human insulin on single-crystal gold surfaces investigated by *in situ* scanning tunnelling microscopy and electrochemistry. Phys. Chem. Chem. Phys. 12, 9999-10011.

[38] Braun, R., Sarikaya, M., Schulten, K., 2002. Genetically engineered gold-binding polypeptides: structure prediction and molecular dynamics. J. Biomater. Sci. Poymer. Edn. 13, 747-757.

[39] Nicholas, J.F., 1965. An atlas of models of crystal surfaces, Gordon and Breach, Science Publishers, Inc., London (UK).

Figure captions

Fig. 1. Current density (in μA cm^{-2}) generated by *G. sulfurreducens* on the different electrode surfaces polarized at +0.2 V *vs.* Ag/AgCl at early times after inoculation (A) and for the total experiment time (B). Inset panel A: a closer view of current generated on platinum electrodes. The batch culture was kept during 25 h and from this time new growth medium was constantly added. Data corresponding to one out of four independent experiments are shown.

Fig. 2. Typical cyclic voltammograms taken at 10 mV s^{-1} after 25 h of in batch culture of the *G. sulfurreducens* on the different anode materials. In each voltammogram dashed lines represent the second cycle. The red dashed lines indicate the steady state current levels that were taken as baselines for calculating the transferred charges. Data corresponding to one out of four independent experiments are shown.

Fig. 3. First derivative plots of cyclic voltammograms (second cycle) shown in figure 2 displaying the midpoint potential of the catalytic redox species involved in the electron transfer process and additional features of the *G. sulfurreducens* biofilm grown on the different anodes after 25 h.

Fig. 4. Cyclic voltammograms taken at 10 mV s^{-1} at 140 h of biofilm growth polarized at +0.2 V *vs.* Ag/AgCl on the different electrodes. Data corresponding to one out of four independent experiments are shown.

Fig. 5. Laser scanning confocal microscopy images of *G. sulfurreducens* biofilms on the different anode surfaces. Working anodes were fluorescently stained using the kit LIVE/DEAD Baclight bacterial viability kit (Invitrogen). Bacteria with intact cell membrane stain green whereas those with damaged membrane fluoresce red. The lateral images are the cross section views along the z-axis reconstructed from the set of optical slides collected at different heights, and the electrode surface would be located on the bottom and right side of each one.

Highlights

1. Electrode crystallographic orientation and nature affect *Geobacter* current generation

2. Gold single-crystals are better substrates than platinum for current production

3. The highest current density is attained with Au(210) electrodes (1442 ±101 μA cm^{-2})

4. The active molecules wiring the biofilm to the electrode are the same in all cases

Table 1. Representative data of the bioelectrocatalytic activity of *G. sulfurreducens* biofilms grown on gold and platinum single-crystals and on a graphite rod[a]

Electrode	*j*max[b] / μA cm^{-2}	pzc[c] or pme[c] ± 0.01 V / V (*vs*. Ag/AgCl)	E_{midp}[d] ± 0.01 / V (*vs*. Ag/AgCl)			$d_{biofilm}$[e] /μm	
			25 h	47 h	140 h	Total	Active
Au(210)	1442 ± 101	-0.09	-0.38	-0.38	-0.35	30 ± 5	25 ± 4
Au(111)	961 ± 94	+0.36	--	-0.39	-0.35	9 ± 2	4 ± 1
Au(110)	944 ± 89	-0.01	-0.39	-0.39	-0.35	11 ± 4	4 ± 1
Pt(111)	658 ± 65	+0.09	-0.39	-0.38	-0.36	8 ± 2	4 ± 1
Pt(100)	518 ± 37	-0.06	-0.39	-0.37	-0.36	9 ± 3	3 ± 1
Pt(110)	343 ± 31	-0.38	-0.39	-0.39	-0.36	7 ± 2	2 ± 1
Graphite	662 ± 37	--	-0.37	-0.36	-0.33	35 ± 8	15 ± 3

[a] Data are the average of four independent experiments.

[b] j_{max}, maximum current density.

[c] The zero charge potential (pzc) for gold crystals has been taken from [26]. For platinum electrodes, the determination of the pzc is complicated by the existence of adsorption processes and the potential of maximum entropy (pme) as determined from laser induced temperature jump experiment represent the best estimation of the pzc if it is assumed that pzc nearly coincides with the pme (for a detailed discussion see [23]). In this case, we use the pme as determined from laser induced temperature jump experiment [23] and extrapolated to the pH of the present study by considering the pH dependence reported in the same work.

[d] E_{midp}, major midpoint potential.

[e] $d_{biofilm}$, measured biofilm thickness.

Figure 1

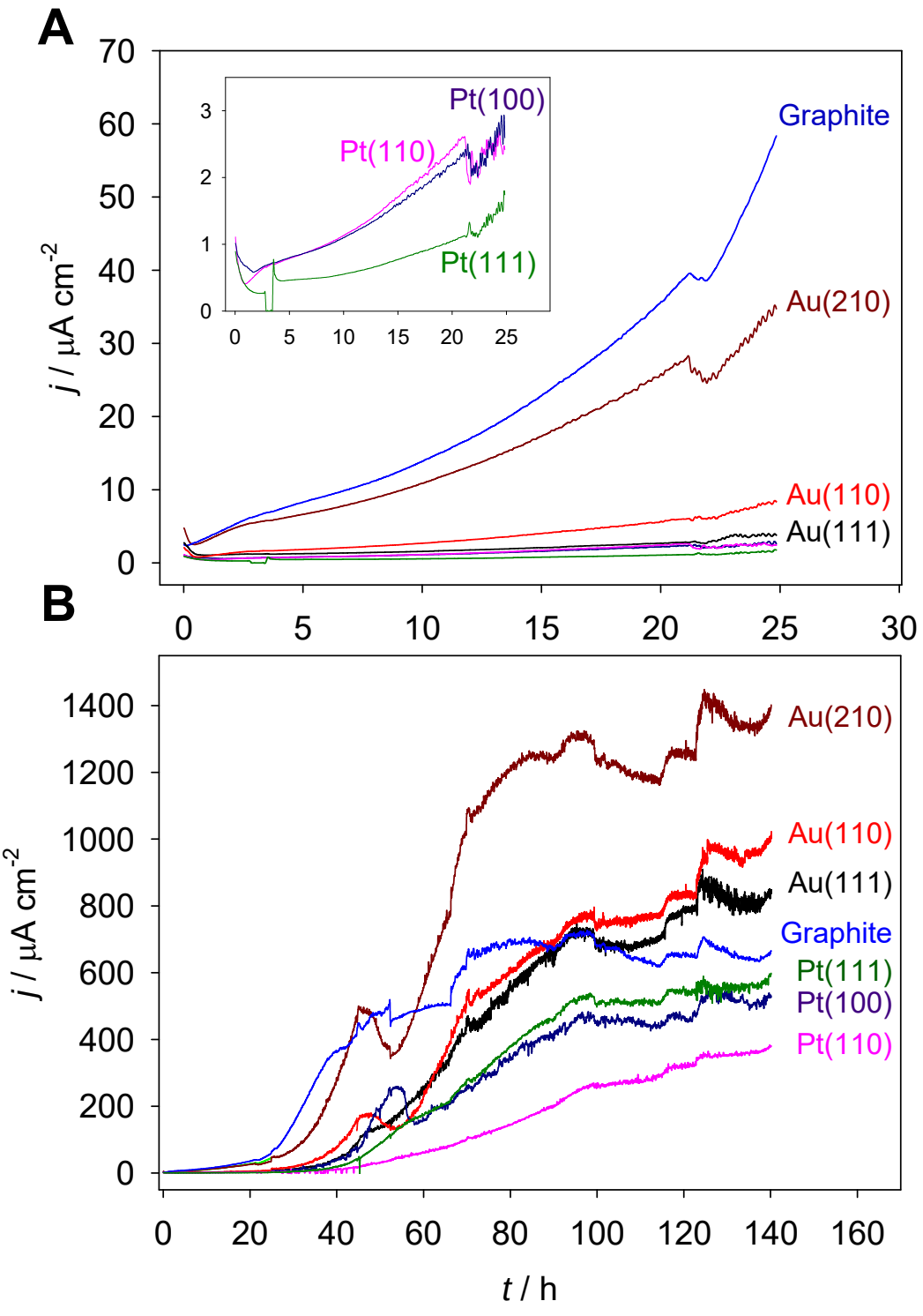

Figure 2

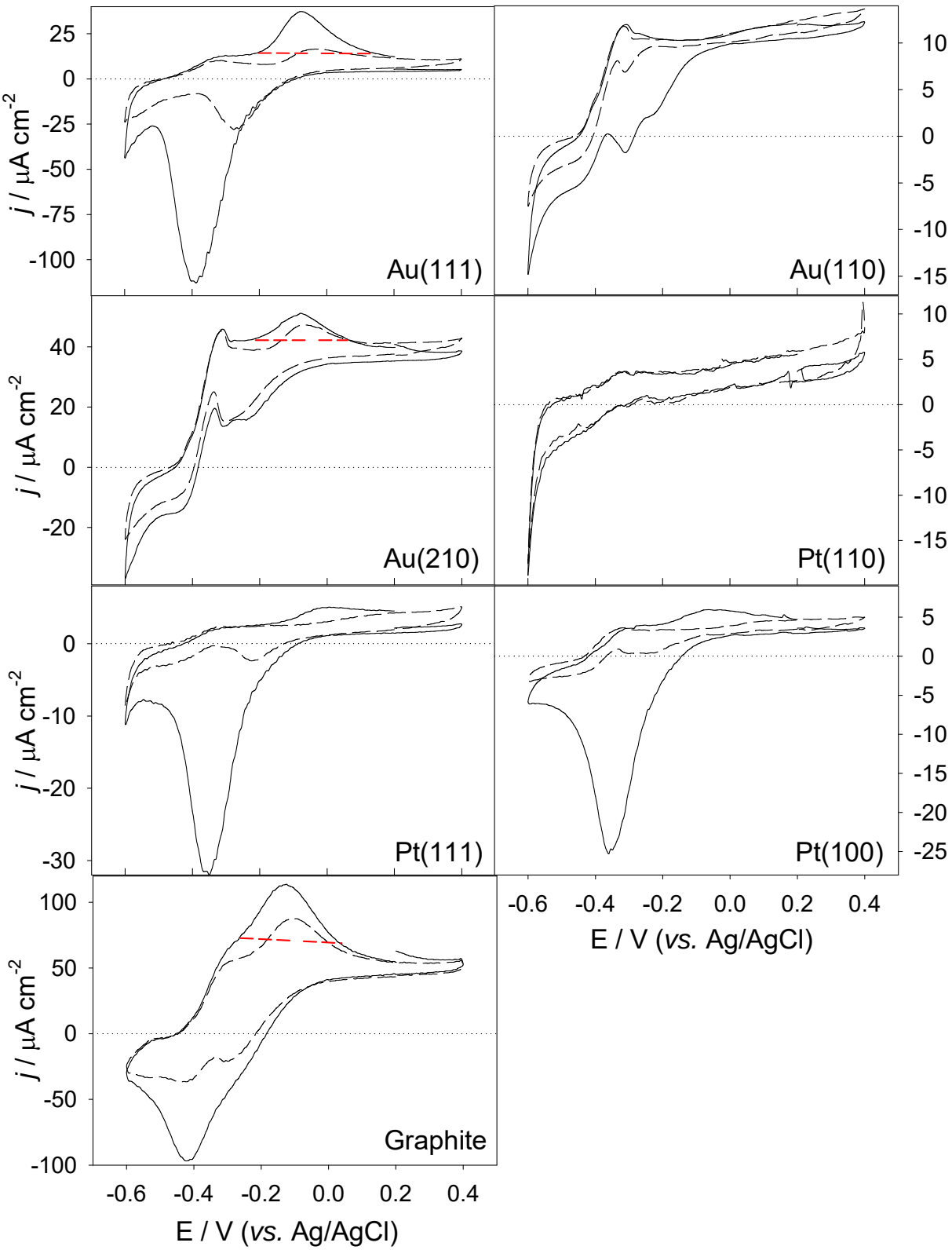
Au(111)
Au(110)
Au(210)
Pt(110)
Pt(111)
Pt(100)
Graphite
j / µA cm-2
E / V (vs. Ag/AgCl)

Figure 3

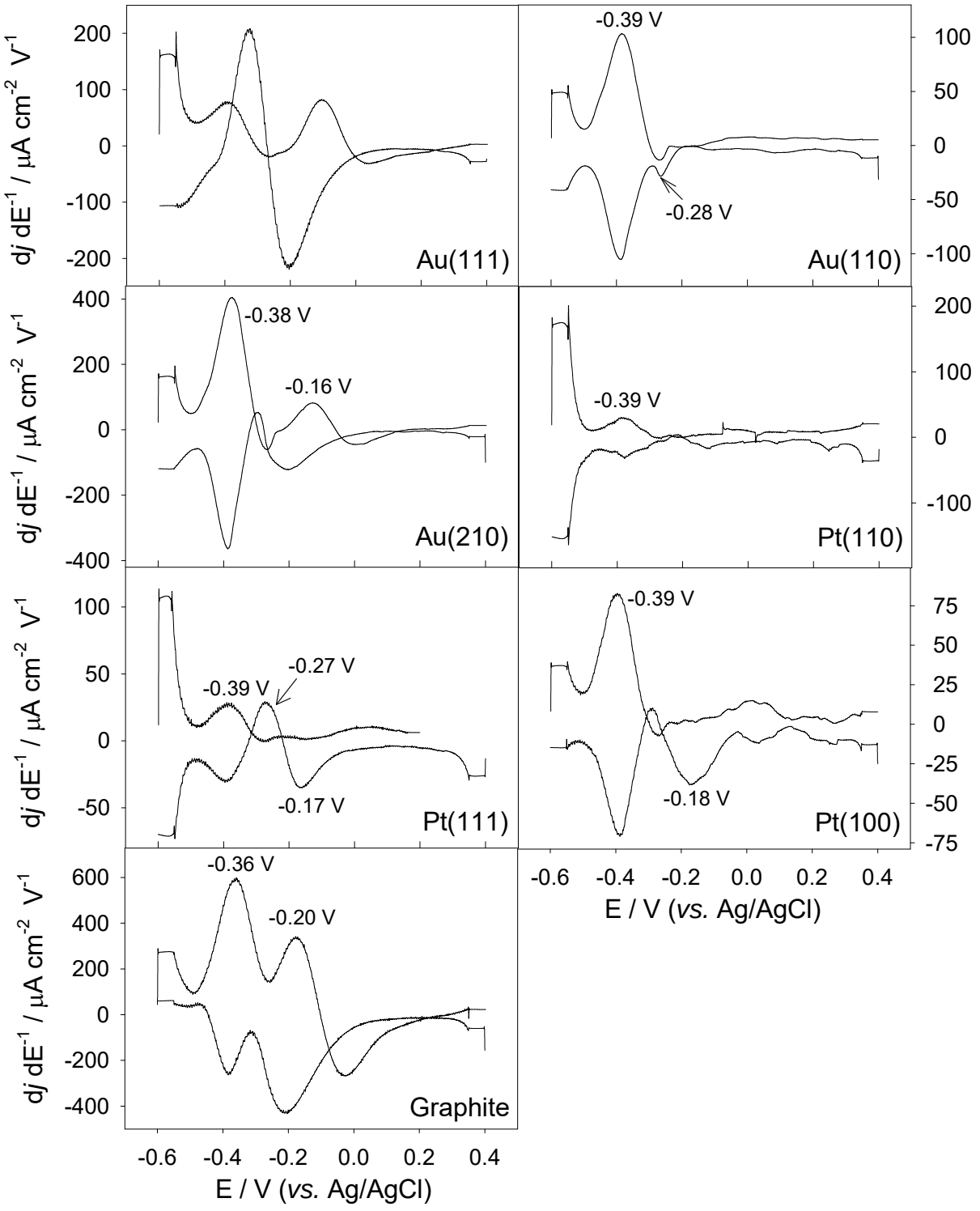
Au(111)
Au(110)
Au(210)
Pt(110)
Pt(111)
Pt(100)
Graphite
-0.39 V
-0.28 V
-0.38 V
-0.16 V
-0.39 V
-0.39 V
-0.27 V
-0.17 V
-0.39 V
-0.18 V
-0.36 V
-0.20 V
dj dE-1 / µA cm-2 V-1
E / V (vs. Ag/AgCl)

Nombre del fichero	Dirección URI Docta
Beatriz_Maestro_18.pdf	https://hdl.handle.net/20.500.14352/93155
Beatriz_Maestro_20.pdf	https://hdl.handle.net/20.500.14352/93157
Beatriz_Maestro_24.pdf	https://hdl.handle.net/20.500.14352/93182
Beatriz_Maestro_25.pdf	https://hdl.handle.net/20.500.14352/93162
Beatriz_Maestro_27.pdf	https://hdl.handle.net/20.500.14352/93188
Beatriz_Maestro_28.pdf	https://hdl.handle.net/20.500.14352/93420
Beatriz_Maestro_29.pdf	https://hdl.handle.net/20.500.14352/93429
Beatriz_Maestro_31.pdf	https://hdl.handle.net/20.500.14352/93196
Beatriz_Maestro_35.pdf	https://hdl.handle.net/20.500.14352/93441
Beatriz_Maestro_36.pdf	https://hdl.handle.net/20.500.14352/93449
Beatriz_Maestro_37.pdf	https://hdl.handle.net/20.500.14352/93649

Nombre del fichero	Dirección URI Docta
Beatriz_Maestro_18.pdf	https://hdl.handle.net/20.500.14352/93155
Beatriz_Maestro_20.pdf	https://hdl.handle.net/20.500.14352/93157
Beatriz_Maestro_24.pdf	https://hdl.handle.net/20.500.14352/93182
Beatriz_Maestro_25.pdf	https://hdl.handle.net/20.500.14352/93162
Beatriz_Maestro_27.pdf	https://hdl.handle.net/20.500.14352/93188
Beatriz_Maestro_28.pdf	https://hdl.handle.net/20.500.14352/93420
Beatriz_Maestro_29.pdf	https://hdl.handle.net/20.500.14352/93429
Beatriz_Maestro_31.pdf	https://hdl.handle.net/20.500.14352/93196
Beatriz_Maestro_35.pdf	https://hdl.handle.net/20.500.14352/93441
Beatriz_Maestro_36.pdf	https://hdl.handle.net/20.500.14352/93449
Beatriz_Maestro_37.pdf	https://hdl.handle.net/20.500.14352/93649